Journal of Photochemistry & Photobiology, A: Chemistry 437 (2023) 114443

Contents lists available at ScienceDirect

Journal of Photochemistry & Photobiology, A: Chemistry

journal homepage: www.elsevier.com/locate/jphotochem

Visible light-induced radical polymerization of vinyl acetate mediated by organo-nickel N_2O_2 Schiff-base complexes

Naralyne M. Pesqueira [a], Camila Bignardi [a], Larissa F. Oliveira [a], Antonio E.H. Machado [b], Valdemiro P. Carvalho-Jr [a], Beatriz E. Goi [a,*]

[a] Faculdade de Ciências e Tecnologia, UNESP – Univ. Estadual Paulista, CEP 19060-900 Presidente Prudente, SP, Brazil
[b] Instituto de Química, Universidade Federal de Uberlândia, P.O. Box 593, Uberlândia 38400-089, Minas Gerais, Brazil

ARTICLE INFO

Keywords:
Photo-OMRP
Radical polymerization
Copolymer
LED irradiation

ABSTRACT

Four nickel(II) complexes with symmetrically substituted N_2O_2 tetradentate Schiff-base ligands, prepared from the 2:1 condensation of 3-*tert*-butyl-salicylaldehyde, and ethylenediamine (**1**), *o*-phenylenediamine (**2**), *1,2-cis, trans*-cyclohexyldiamine (**3**), or 1,3-diaminepropane (**4**), were synthesized. These Ni^{II} Schiff-base complexes (**1**–**4**) were used as control agents for the polymerization of vinyl acetate (VAc) photoinitiated by diphenyl(2,4,6-trimethylbenzoyl)phosphine oxide (TPO) according to a photoinduced organometallic-mediated radical polymerization (photo-OMRP) mechanism. All complexes presented good control ability, although the polymerization mediated by **3** showed the best control over molecular weight (M_n matching $M_{n,th}$) and dispersity ($Đ < 1.50$). The livingness of the polymers has been confirmed by LED on and LED off experiments, the polymerization stopped immediately, and no monomer conversion was observed during the light-off period, indicating a negligible concentration of the active radical in the dark. Further, to demonstrate the living nature of this system, block copolymers of poly(vinyl acetate)-*b*-poly(methyl acrylate) were synthesized using the sequential visible-light-induced process. Kinetic results and computational investigations supported the activation/deactivation equilibrium exerted by complexes **1**–**4**, which occurred on only one face of the complexes via reversible deactivation (RD) mechanism.

1. Introduction

Polymeric materials have shaped the modern world and become a part of all facets of society. While commodity plastics are undoubtedly important, polymeric materials have also emerged to address challenges in the coating, biomedical, electronic and energy-storage fields [1–3]. Radical polymerization is the most widely used mechanism to synthesize polymer networks because of its broad monomeric scope and functional group tolerance. The conventional step- or chain-growth polymerizations show limited ability to control macromolecular structures [1]. These polymerizations are often characterized by generation of an active initiating species, propagation by addition of monomer units, and eventual termination of polymer chains [1,2]. The occurrence of unavoidable and irreversible chain transfer/termination reactions leads to broad chain length distributions that are inactive with respect to further chain growth. Thus, the properties of polymer materials and the controlled introduction of functional building blocks are limited [3].

To overcome this challenge, radical controlled polymerizations have been proved effective in imparting a high level of control over desirable polymer characteristics, while providing access to a wide array of materials [4–6]. Specifically, reversible deactivation radical polymerization (RDRP) – formerly known as living radical polymerization – is a family of reactions discovered in the 1990s that has become increasingly important over the past few decades, showing wide control under different conditions using transition metal complexes [7–10]. These reactions have received large attention because of their capability to polymerize less active monomers (LAM), such vinyl acetate (VAc), and more active monomers (MAM), such methyl and butyl acrylates [10]. The equilibrium principle between a growing radical chain and a dormant species is used to reduce chain-breaking reactions and ensure quantitative initiation. Therefore, this dynamic equilibrium between dormant species and growing radicals is termed RDRP, resulting in excellent control over molecular weights, polydispersity, and functionality [11].

* Corresponding author.
E-mail address: beatriz.goi@unesp.br (B.E. Goi).

https://doi.org/10.1016/j.jphotochem.2022.114443
Received 28 June 2022; Received in revised form 4 November 2022; Accepted 20 November 2022
Available online 23 November 2022

These reactions can occur through cleavage of the initiator under different stimuli, such as thermal, redox or photo cleavage [12,13]. The photochemical production of primary radicals requires low temperatures (10–40 °C), unlike thermal free-radical initiators, which generally occur at temperatures >40 °C [4,14]. Consequently, photopolymerization can be carried out at very low temperatures, resulting in absence of the chain transfer processes that leads to branched macromolecules. Photopolymerization at low temperatures yields the low-energy stereospecific polymeric species [15]. However, the equilibrium of organometallic-mediated radical polymerization (OMRP) is importantly suitable to regulate highly reactive propagating radical species, since their activation relies only on the dissociation energy of the metal–carbon bond in the dormant state. Notwithstanding, OMRP possesses present a distinct advantage in copolymerization because of the capability of the metal complex to activate unreactive bonds, significantly expanding the monomer scope [6].

The ability of OMRP to yield advanced polymeric materials with predetermined molecular weights, low polydispersity indexes, and controlled topology, composition and functional groups makes this polymerization increasingly valuable. Various metal complexes are used to control OMRP, including Co [16], Fe [17], Mo [18], Rh [19], and other compounds formed by porphyrins, Schiff bases, and α-diimine ligands [9,16,20,21].

In the past decades, transition metal complexes containing N_2O_2 Schiff bases have been intensively studied in the fields of organometallic chemistry and materials science [22,23]. Nickel complexes bearing N_2O_2 Schiff bases have stood out in the field of catalysis because of their properties, as well as of their application as catalysts or electrocatalysts in numerous organic redox reactions [24–26]. This attention derives from the possibility of forming electrochemical stable oxidized or reduced complexes, which enables their utilization in electrocatalytic oxidation and reduction treatment systems [27]. In contrast to other metal ions, the Ni^{II} ion is diamagnetic (low-spin) in the square planar coordination environment provided by most Salen complexes [28]. This type of Ni^{II} Schiff base complexes can also be applied in polymerization reactions. Silva et al. applied Ni^{II} Schiff-base complexes in the OMRP of VAc, and found that these complexes show good control capability (Đ ≈ 1.2) [28]. Our research group is experienced in this type of polymerization under thermal stimuli using Co^{II} [21,29,30], Mn^{II} [31], or Ni^{II} [28] as mediating agents. More recently, we have applied Co^{II} Schiff-base complexes in the photo-OMRP of acrylates and verified that light was a good cleavage source [32,33]. Motivated by the behaviour of the Ni^{II} Schiff-base complexes, we decided to apply four Ni^{II} complexes (Fig. 1) coordinated to tetradentate Schiff bases to the photo-OMRP of VAc using diphenyl(2,4,6-trimethylbenzoyl)phosphine oxide (TPO) as initiating agent.

2. Experimental

2.1. General remarks

All reagents were purchased from Aldrich Chemical Co. All reactions and manipulations were performed under nitrogen atmosphere using standard Schlenk techniques. Vinyl acetate (VAc) and methyl acrylate (MA) were washed with 5 % NaOH solution, dried over anhydrous $MgSO_4$, degassed in several freeze-thawing cycles, and then distilled in CaH_2 and stored at −18 °C under nitrogen atmosphere. $NiCl_2$ was carefully dried in a reaction flask under reduced pressure (0.5 torr) using a hair dryer until it turned from green to yellow. Ethylenediamine, *o*-phenylenediamine, 1,2-*cis,trans*-cyclohexyldiamine, 1,3-diaminepropane, and TPO were used as acquired. The *tert*-butylsalicylaldehyde was synthetized as described in the literature [34]. The Schiff base ligands (3,6-*ditert*-butyl-N,N′-ethylenebis(salicylimine) (L_1H_2), 3,6-*ditert*-butyl-N,N′-*o*-phenylene(salicylimine) (L_2H_2), 3,6-*ditert*-butyl-N,N′-cyclohexylbis(salicylimine) (L_3H_2) and 3,6-*ditert*-butyl-N,N′-1,3-propanbis(salicylimine) (L_4H_2)) and the complexes **1**–**3** were synthetized as described in the literature [35–37]. The synthesis and characterization of the ligands and complexes **1**–**3** are reported in the Supporting Information.

2.2. Analyses

Elemental analyses were performed on a Perkin-Elmer CHN 2400 instrument. The infrared spectra were obtained on a Perkin Elmer Frontier instrument equipped with a diamond ATR module, collected between 4000 and 250 cm^{-1} at a scan rate of one spectrum every 64 s with a 2 cm^{-1} resolution at 298 K. The ^1H and $^{13}C\{^1H\}$ NMR spectra were obtained in $CDCl_3$ at 298 K on an Agilent MR 400 Ultrashield spectrometer operating at 400.13 and 100.61 MHz, respectively. The obtained chemical shifts were reported in ppm relative to the high frequency of TMS. Molar conductance of the complexes was measured in CH_2Cl_2 solution at room temperature using a Systronics 304 Digital Conductivity Meter. Conversion was determined from the concentration of residual monomer measured by infrared spectra using a Perkin Elmer Frontier instrument equipped with a diamond ATR module. The molecular weights and molecular weight distribution (MWD) of the polymers were determined by gel permeation chromatography using a Shimadzu Prominence LC system equipped with a LC-20AD pump, a DGU-20A5 degasser, a CBM-20A communication module, a CTO-20A oven at 40 °C, and a RID-10A detector equipped with two Shimadzu columns (GPC-805: 30 cm, Ø = 8.0 mm). Retention time was calibrated with standard monodispersed polystyrene using HPLC-grade THF as eluent at 40 °C with a flow rate of 1.0 mL min^{-1}. Đ is M_w/M_n. Theoretical molecular weights were calculated without considering the end groups according to the following equation: $M_{n,th} = ([Monomer]_0/[Ni]_0) \times Conversion \times M_{n\ monomer}$. The electronic spectra were recorded on a Shimadzu model UV-1800 spectrophotometer using 1 cm path length quartz cells. CH_2Cl_2 solutions of the complexes at 0.2 mM concentration were used for these measurements. Electrochemical measurements were performed using an Autolab PGSTAT204 potentiostat with a stationary platinum disk and a wire as working and auxiliary electrodes, respectively. The reference electrode was Ag/AgCl. The measurements were performed at 25 °C ± 0.1 using a 0.1 mol/L of *n*-Bu_4NPF_6 solution in CH_2Cl_2 as supporting electrode. The $E_{1/2}$ values were the arithmetic average of the anodic and cathodic potential peaks: $(E_{p,a} + E_{p,c})/2$.

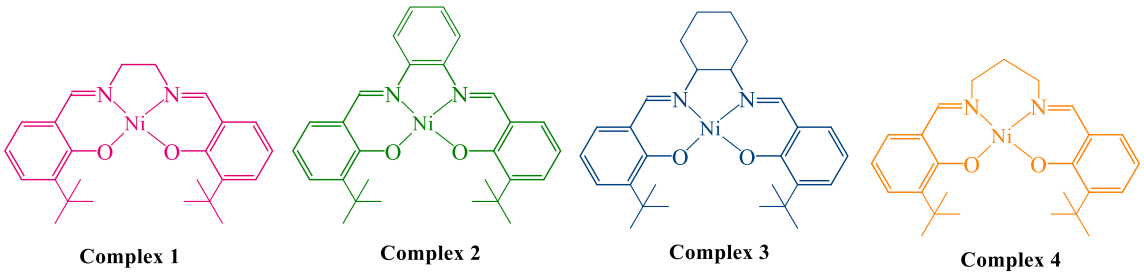

Fig. 1. Structure of Ni^{II} Schiff-base complexes **1**–**4**.

2.3. Synthesis of complex 4

The solution of ligand L_4H_2 (0.394 g, 1 mmol) in methanol (30 mL) with NaOH were added to a Schlenk flask containing the anhydrous nickel (II) chloride (0.119 g, 1 mmol) and stirred overnight under reflux (65 °C). The reaction mixture was then concentrated and dried in vacuum. The resulting powders were filtered and recrystallized in dichloromethane/hexane (1:2 v/v) solution. Yield: 65 %. a) UV–vis CH_2Cl_2 $\lambda_{max(n)}$ (nm), $\varepsilon_{max(n)}$ [mol L^{-1} cm^{-1}]: $\lambda_{max(1)}$ (227) $\varepsilon_{max\ (1)}$ [1672], $\lambda_{max(2)}$ (252) $\varepsilon_{max\ (2)}$ [20,915], $\lambda_{max(3)}$ (271) $\varepsilon_{max\ (3)}$ [23,860], $\lambda_{max(4)}$ (354) $\varepsilon_{max\ (4)}$ [3790], $\lambda_{max(5)}$ (424) $\varepsilon_{max\ (5)}$ [3195], $\lambda_{max(6)}$ (500) $\varepsilon_{max(5)}$ [280]; b) FTIR (cm^{-1}): 3020 ν(aromatic C—H), 2942 ν(sp^3 C—H), 1630 ν(C═N), 1546 ν(C═C), 1312 ν(C—O), 761 ν(sp^3 C—H) 478 ν(Ni—N), 370 ν(Ni—O); c) Anal. Calc. for $C_{25}H_{32}NiN_2O_2$: C: 66.54; H: 7.15; N: 6.21; Found: C: 66.50; H: 7.20; N: 6.20; d) MALDI-TOF: (*m/z*) 451.26437; d) Molar conductance: 0.67 μs^{-1} cm^2 mol^{-1}; e) ^1H NMR ($CDCl_3$ δ/ppm): 1.39 (s, 18H, —$C(CH_3)_3$), 1.87–1.82 (m, 2H, —CH_2—), 3.59 (t, $J = 7.1$ Hz, 4H, CH_2), 6.47 (t, $J = 7.5$ Hz, 6H, Ar—H), 6.92 (dd, $J = 7.8$, 1.8 Hz, 2H, —NH═C—), 7.20 (s, 2H, —CH═N).

2.4. Computational details

The structures of the compounds under study were optimized using the density functional theory (DFT) at the level of the hybrid functional PBE0 [38], implemented in Gaussian 09 [39], using the DGDZVP basis set [40,41]. The optimizations and calculation of the vibrational frequencies were conducted with no symmetry constraints. As the Ni^{II} complexes under study are low-spin four coordinate with distorted square planar coordination environment compounds ($S = 1/2$) [42,43], all calculations were performed considering a multiplicity equal to 4. After optimization, in all cases, $<S2> = S(S + 1) = 3.75$, suggesting the desirable non-existence of spin contamination in the generated orbital-based wave functions. For the Ni^{III} complexes formed by the coupling between the Ni^{II} complex and the vinyl acetate radical, multiplicity was defined as unitary. Several previously conducted studies have reported DFT calculations of CMRP dormant species models [44–49]. Here, aiming to reproduce the experimental conditions, the simulations involving these compounds were also performed under the solvation condition. To this end, the previous structure was reoptimized using the IEFPCM model [39] to build a dielectric continuum with the characteristics of dichloromethane in a self-consistent reaction field procedure .[39] The structure of the product of coupling between the Ni^{II} complexes and the VAc radical was optimized only under the solvation condition.

2.5. General procedure for VAc photo-OMRP

The photopolymerization procedure for VAc was as follows: a mixture solution was obtained by adding the Ni^{II} complexes, TPO, dichloromethane (0.5 mL), and VAc (5.0 mL, 21.6 mmol) to a dried Schlenk flask (25 mL) with a stir bar. The solution was deoxygenated through three standard freeze–pump–thaw cycles, flame-sealed, and placed in a stirring apparatus under LED irradiation (10 W/cm^{-2} at 390 and 400–800 nm). The samples were regularly collected from the medium using a nitrogen flushed syringe. The monomer was evaluated by FTIR to determine conversion and *SEC*-THF to obtain molecular parameters using PMMA standards.

2.6. Copolymerization general procedure

Copolymerization of VAc and MA was carried out in CH_2Cl_2 solution at 25 °C under nitrogen atmosphere using TPO (0.0121 mmol) as radical initiator and the complexes **1**–**4** as mediators (0.0362 mmol). A known volume of VAc (2.0 mL) was transferred to the reaction tube and the contents were degassed through three freeze–pump–thaw cycles. The tubes were then tightly sealed and placed in a photo reactor at the controlled temperature of 25 °C. After the desired interval, the MA solution (1.4 mL) was poured into the reaction flask. The precipitated polymers were filtered, purified by reprecipitation, and then dried at 60 °C for 12 h.

2.7. Results and discussion

A series of four Salen-type Schiff-base ligands, L_1H_2–L_4H_2, and their respective Ni^{II} complexes were synthesized (Scheme 1). The reaction of 3-*tert*-butylsalicylaldehyde with four diamines (ethylene, *o*-phenylene, cyclohexyl and propanediamine) in methanol gave the desired symmetric tetradentate Schiff base ligands in high yields and purity. Ni^{II} complexes with tetradentate Schiff base ligands were prepared by treating an methanolic solution of the appropriate ligand (1 equiv.) and NaOH (2 equiv.) with anhydrous $NiCl_2$ (1 equiv.). After synthesis, the complexes **1**–**4** were fully characterized by means of FTIR and UV–vis spectroscopy, elemental analysis, cyclic voltammetry, computational methods, and mass spectrometry.

The ^1H NMR spectrum of the complex **4** shows the disappearance of the signal corresponding to OH moieties, observed at 14.02 ppm in the L_4H_2 spectrum (Figs. S4 and S5). Furthermore, the signals related to the phenyl rings, found in the range 6.82–7.35 ppm for the free ligand, suffer a shielding effect upon complexation to lower δ in the range of 6.47–7.18 ppm. The same behaviour is observed for the protons bonded to C═N which are found in 8.39 ppm for the free ligand and 7.20 ppm for the complex. [50] Comparing the FTIR spectra of the ligand L_4H_2 and its respective complex **4** (Fig. S9), the ν(C—O) stretching frequencies red-shifted to 1230 cm^{-1} and the bands around 3150 cm^{-1} corresponding to ν(O—H) disappeared in the FTIR spectrum of the complex, indicating that the hydroxyl group participated in the coordination process. New vibration bands were noticed in the spectrum of the complex at wave number ranges of 448 and 383 cm^{-1}, assigned to (Ni—N) and (Ni—O) vibrations, respectively. [50] Data on the absorption spectra of the free LH_2 Schiff-base ligand and their respective complexes **1**–**4** were collected in CH_2Cl_2 (Fig. 2). The bands around 230, 256 and 330 nm attributed to the π → π* and n → π* transitions in the benzene ring or azomethine (—C═N) groups were found for LH_2. [51] Upon complexation, these bands were shifted to a lower wavelength region at 227 and 252 nm (π → π*) and 271 nm (n → π*), suggesting the coordination of azomethine nitrogen with the Ni^{II} ion. Four bands were observed complexes **1**–**4**, around 451, 415, 264 and 231 nm. The band with lower molar absorption coefficient at 500 nm, corresponds to *d-d* transitions in the Ni^{II} ion. The absence of bands around 600 nm indicates that the complex presents a square planar d^8 geometry. [52,53] Mass spectrometry was successfully used to confirm the molecular ion peak of complex **4** (Fig. S13). The recorded mass spectrum of this complex revealed a molecular ion peak, which strongly confirms the proposed formula for it, as 451.26437 *m/z*. This value was in good agreement with the composition proposed for the nickel complex. With a view to studying the electrolytic nature of the complexes **1**–**4**, their molar conductivities were measured in CH_2Cl_2 solution at 10^{-3} mol L^{-1}. The molar conductivity values found for these complexes are in the range of 0.35–0.67 $\mu s^{-1}cm^2$ mol^{-1} at room temperature, indicating their non-electrolytic nature.

Additional characterizations of complexes **1**–**3** by theoretical studies were necessary to complete the early presented studies [36,37], to better understand their reactivity in the current purpose. Thus, optimized geometries for complexes **1**–**4** were obtained by DFT using PBE0 level of theory in combination with the DGDZVP basis set (Fig. 3). Calculated selected bond distances and bond angles are listed in Table S1. The two Ni—N iminic and Ni—O phenolic bond lengths are similar for complexes **1**–**4**, with variation smaller than 0.0306, 0.0297, 0.0154 and 0.0073 Å for Ni—N(1), Ni—N(2), Ni—O(1) and Ni—O(2), respectively, whereas the calculated bond angles show considerable differences, mostly driven by a conformation change in the Schiff-base bridge. In the structure of these complexes, the Schiff-base ligand (L_1H_2-L_4H_2) acts as a N_2O_2 donor

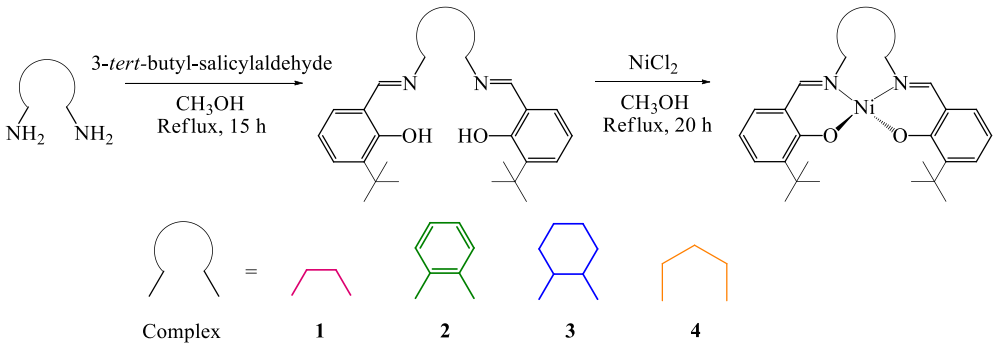

Scheme 1. Synthesis of the LH_2 ligands and their respective Ni^{II} complexes.

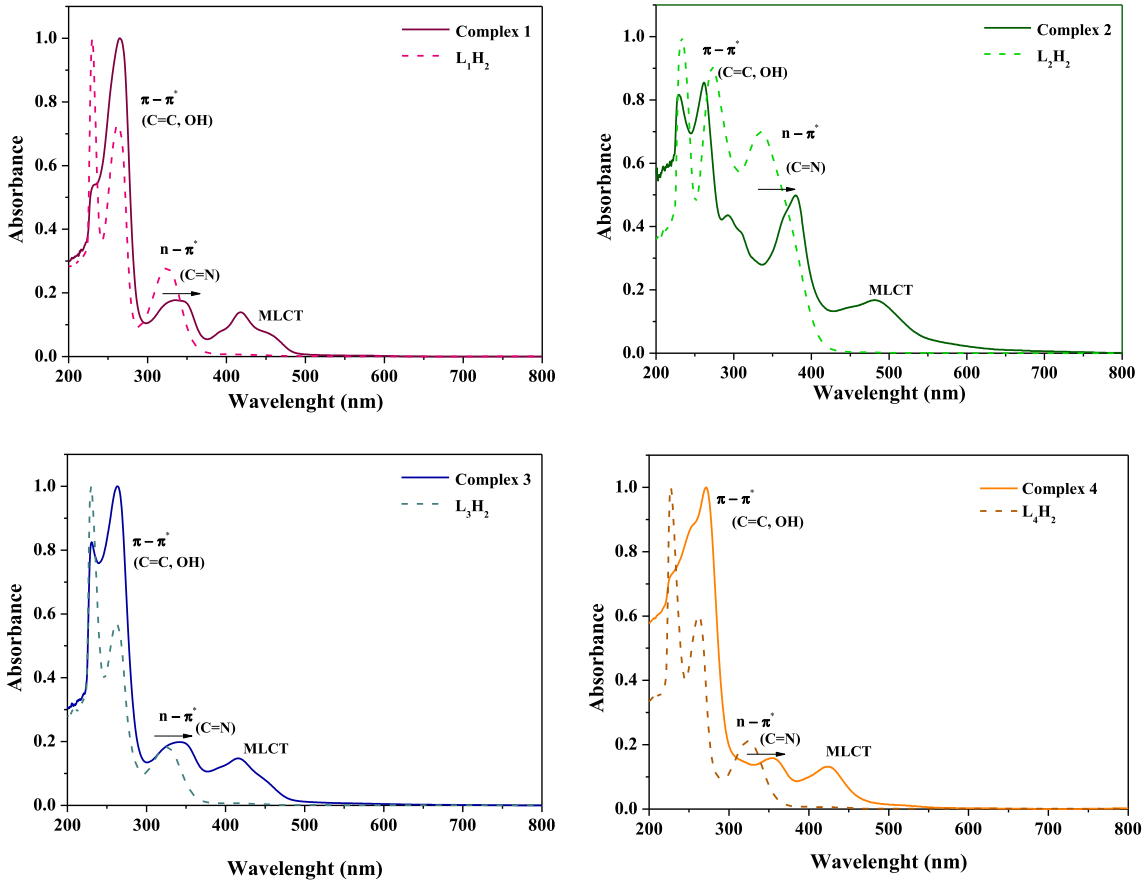

Fig. 2. UV–vis spectra for Complexes **1**–**4** and Ligands L_1H_2-L_4H_2 in CH_2Cl_2 at 25 °C; [Ni] = 1 × 10^{-4} mol/L.

set, and is coordinated to the metal via two oxygen atoms (O1 and O2) and two iminic nitrogen (N1 and N2) atoms. The value of the *trans* angles around the Ni^{II} center changes from 180° to [171.041–176.574°], whereas the value of the *cis* angles deviates from the ideal angle of 90° [85.665–94.215°]. Thus, complexes **1**–**4** present a square planar distorted coordination geometry (Fig. 3). All the bond lengths and angles around the Ni^{II} center are within the normal range reported for similar coordination compounds [16,19].

Aiming to study the electrochemical behaviour of complexes **1**–**4**, cyclic voltammetry measurements were performed in CH_2Cl_2 solutions using *n*-Bu_4NPF_6 0.1 mol/L as supporting electrolyte at 25 °C. The cyclic voltammograms of **1**–**4** are shown in Fig. 4, and the pertinent data are presented in Table S2. The $E_{1/2}$ values for complexes **1**–**4** indicate that the number of C atoms on the imine bridge influences the potentials found of 0.90, 0.99, 0.89 and 0.79 V for complexes **1**–**4,** respectively. The electrochemical reversibility of the $Ni^{II/III}$ redox pair for photo-OMRP is extremely important to support the RDRP mechanism. Thus, the electrochemical reversibility of complexes **1**–**4** was initially evaluated by calculating the potential difference (ΔE_p) values and then comparing them with the ΔE_p value of the ferrocene as the reference obtained under the same experimental conditions. Since the complexes **1**–**3** showed ΔE_p values lower than that of ferrocene, whereas for complex **4** was slightly larger than that of ferrocene. Another reversibility criterion is that the anode/cathode peak current ratio should be close to one and independent of the scan rate. The I_{ap}/I_{cp} values for complexes **1** and **3** were higher to that expected for a reversible process, while the values for complexes **2** and **4** were close to one (Table S2). In all cases, the intensity of the peaks increased with the scan rate. Simultaneously, cathodic peaks shifted to more negative potentials while anodic peaks shifted to more positive potentials. The linearity of I_p vs $v^{1/2}$ plots

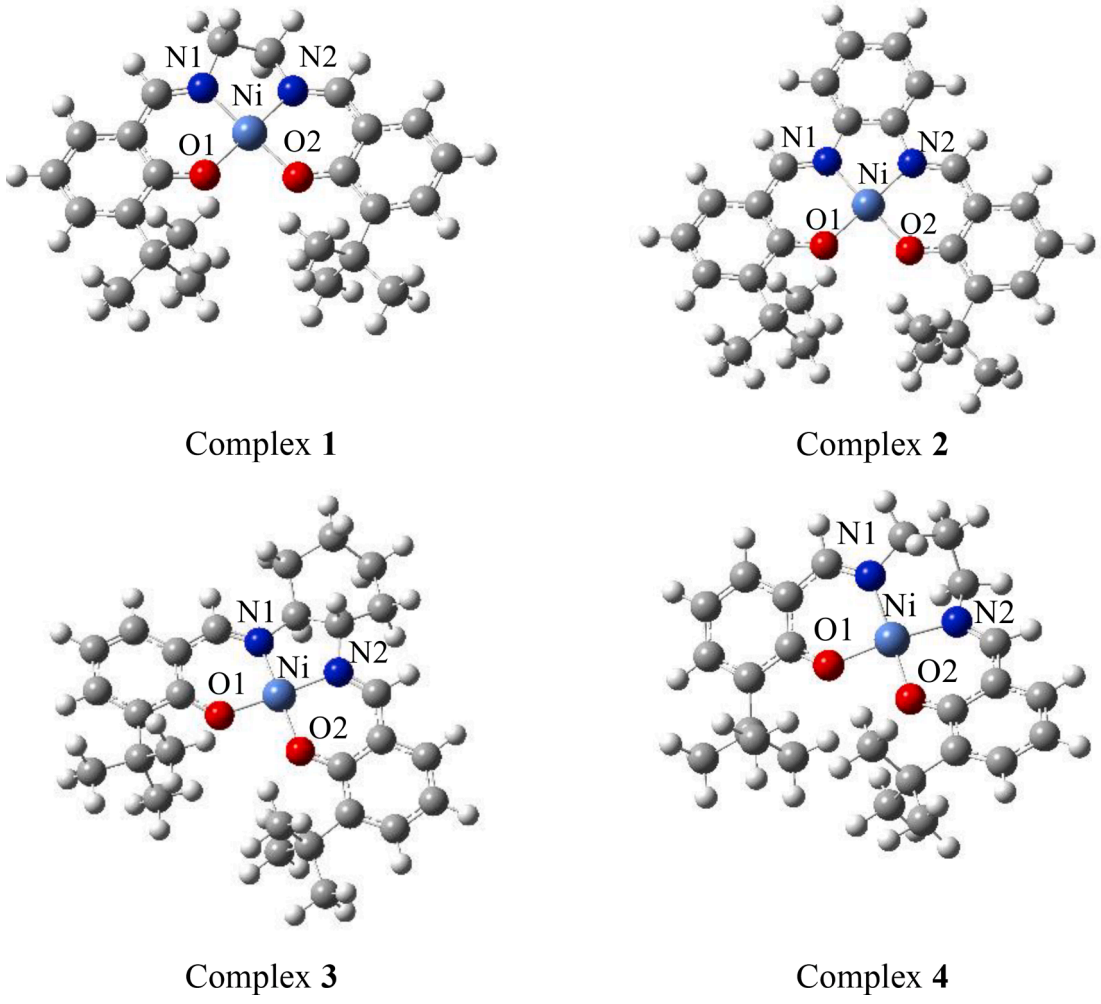

Fig. 3. Optimized geometries in the gas phase for complexes **1**–**4** obtained by DFT using the PBE0 level of theory in combination with the DGDZVP basis set.

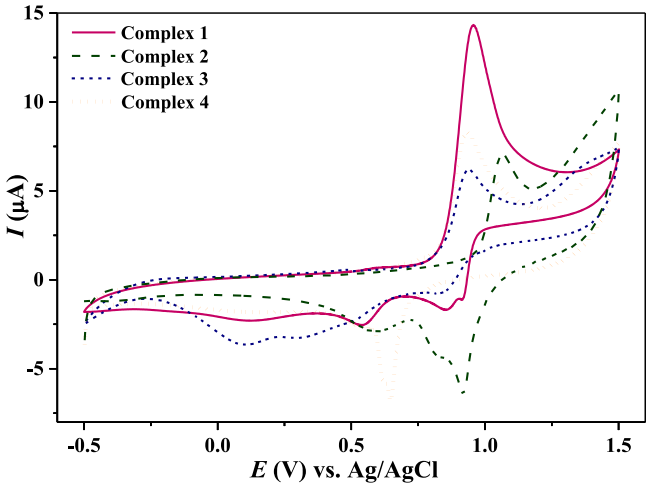

Fig. 4. Cyclic voltammetry of complexes **1**–**4** from 1 × 10^{-3} mol/L CH_2Cl_2 solutions and *n*-Bu_4NPF_6 0.1 mol·L^{-1} vs Ag/AgCl; obtained at 100 mV·s^{-1} at 25 °C.

demonstrates that mass transport of these complexes to the electrode surface is diffusion controlled (Figs. S14-S17). The voltammetric features show that the $Ni^{III/II}$ interconversion for the complexes **1**–**4** is electrochemically quasi-reversible in fast and lower scan rates.

2.8. Photo-OMRP

The photo-OMRP of VAc was conducted using complexes **1**–**4** as control agents in the presence of TPO under LED irradiation. The LEDs used were 390 and 400–800 nm, with 10 W cm^{-2} at 25 °C. The photo-induced polymerization was studied under different conditions. First, a control experiment was conducted in the dark using TPO and VAc, and no conversion was observed after 30 h. A second experiment was performed under LED irradiation with 400–800 nm using VAc and complexes **1**–**4**, and again no conversion was observed. Subsequently, an experiment was developed using VAc and TPO under the LED irradiation of 390 nm, and 95 % conversion was reached after 5 h, with Đ = 3.0. The aforementioned experiments suggest that formation of radicals by TPO cleavage do not occur under purely thermal conditions. In addition, a last experiment was performed in the presence of the Ni^{II} complexes and only under LED irradiation for 24 h, and no polymerization occurred, indicating that the 400–800 nm LED wavelength was needed for the R-Ni^{III} bond cleavage to occur. To investigate the control capability of complexes **1**–**4** in the VAc polymerization, they were studied with different molar ratios, as shown in Table 1. When polymerization was conducted with both TPO and complexes **1**–**4** under LED irradiation, the obtained polymers showed controlled M_n and narrow MWD, which are shown in Table 1. From the data presented in Table 1, it is possible to observe that complexes **2** and **3** showed the best Đ values under all conditions, while complexes **1** and **4** were agents with smaller capability to control polymerization. This investigation also showed that the controllability of the polymerization was affected by the molar ratio

Table 1
Summary of results of the photo-OMRP of VAc with complexes **1**–**4** at different [VAc]/[Ni^{II}]/[TPO] molar ratios after 22 h.[a]

Entry	Complex	Molar ratio [VAc]/[Ni^{II}]/[TPO]	Conv. (%)	$M_{n,GPC}$ ($\times 10^3$)	$M_{n,th}$[b] ($\times 10^3$)	Đ
1	1	600/1/0.5	80	40	41	1.4
2	2	600/1/0.5	34	15	18	1.1
3	3	600/1/0.5	43	23	22	1.2
4	4	600/1/0.5	71	36	37	1.2
5	1	900/1/0.5	79	40	61	1.5
6	2	900/1/0.5	40	23	31	1.1
7	3	900/1/0.5	72	34	56	1.4
8	4	900/1/0.5	70	41	54	1.2
9	1	600/1.5/0.5	85	39	29	1.3
10	2	600/1.5/0.5	20	25	6.9	1.1
11	3	600/1.5/0.5	60	24	21	1.2
12	4	600/1.5/0.5	41	34	14	1.1
13	1	900/1.5/0.5	72	50	37	1.3
14	2	900/1.5/0.5	23	37	12	1.1
15	3	900/1.5/0.5	37	31	19	1.1
16	4	900/1.5/0.5	25	46	13	1.1

[a] All polymerizations were conducted under LED irradiation (10 μW cm^{-2} at 390 and 400–800 nm) at 25 °C.
[b] $M_{n,th} = [VAc]_0/[Ni^{II}]_0 \times MVAc \times Conv.$.

between the Ni^{II} complexes and the monomer. Polymers with controlled M_n and narrow MWD (Đ = 1.2) were obtained using a molar ratio between complexes **1**–**4** and VAc of 1.5/900, showing reasonable conversion values (Fig. S18). According to the literature [32], the constant rate of the polymerization increases with a higher concentration of monomer. The induction period was lower when increasing the VAc molar ratio. This can be assigned to the greater concentration of monomeric radicals formed, which enables faster radical trapping by the Ni^{II} complex, resulting in an overall improved efficiency.

Interestingly, the results displayed in Fig. 5 show a typical induction period in all polymerization experiments. The induction period indicates the need for some time to establish the dynamic equilibrium between the active propagating radicals and the dormant species, which resulted in the slow formation of the Ni—C bond. After the induction time, linear pseudo-first order kinetic behaviour for complexes **1**–**4** with k_{app} of 3.0 $\times 10^{-4}$, 8.9 $\times 10^{-5}$, 1.4 $\times 10^{-4}$ and 7.7 $\times 10^{-5}$ s^{-1}, respectively, was observed throughout the polymerization, indicating constant concentration of propagating radicals.

Aiming to study the kinetics of the photo-OMRP of VAc mediated by complexes **1**–**4**, we decided to investigate the conversion degree and the respective polymerization rate by FTIR spectroscopy in conjunction with Attenuated Total Reflection (ATR), monitoring the band of the olefin in the VAc monomer at 1647 cm^{-1}. This procedure was conducted as described in the literature for the calculation of conversion and rate of polymerization (R_p) [32,33]. Fig. 6 illustrates the R_p evolution as a function of conversion for polymerization of VAc mediated by complexes **1**–**4**. The R_p values increase with increasing VAc conversion, reaching a maximum of 65 % for complex **1** and ~25–37 % conversion for complexes **2**–**4**. For complexes **2**–**4,** there was an increase in the R_p curve, whereas for **1** a slow-down was observed after reaching a maximum, which is associated to the lower mobility resulting from the formation of large polymer chains. As the solution becomes gelled with a conversion of 65 %, the polymer chain interactions are no longer negligible and contribute to decreased molecular mobility. The maximum rate of polymerization, $R_{p(max)}$, is given by the maximum R_p curve. $R_{p(max)}$ values decrease in the following order: **1** > **3** > **2** > **4**. Conversion of 65, 35, 23 and 25 % with $R_{p(max)}$ of 3.54 $\times 10^{-5}$, 1.76 $\times 10^{-5}$, 1.14 $\times 10^{-5}$ and 1.10 $\times 10^{-5}$ mol kg^{-1} s^{-1} is observed, respectively.

The polymerization of VAc was then initiated by complexes **1**–**4** using a molar ratio [VAc]/[Ni^{II}]/[TPO] = 900/1.5/0.5 at 25 °C under LED irradiation. In all the cases, the molecular weight of polyVAc increased with the monomer conversion (Fig. 7). $M_{n,exp}$ values increased linearly with conversion in all cases. The molecular weight matched theoretical values with low Đ values (Đ = 1.1) for complex **3**, whereas $M_{n,exp}$ values were higher than the theoretical ones for complexes **1**, **2**, and **4**. The controlling ability in the VAc photo-OMRP can be related to the electrochemical properties of the complexes **1**–**4.** This correlation is possible due to the OMRP equilibrium which involves a redox process. Therefore, it is important to consider the number of members in the ring between the diimine ligand and the Ni center. For complexes **1**–**3**, that present a five-membered ring, a correlation between the $E_{1/2}$ values and the discrepancy between theoretical and experimental molar weight was noted. The increase of the electron-donating ability, reflected by lower $E_{1/2}$ values, induced a better polymerization control, supported by the good agreement between experimental and theoretical molecular weight. In contrast, for complex **4,** which shows a six-membered ring, the steric factors involved should be considered. Gel permeation chromatography (GPC) traces show that the entire molecular weight distribution (MWD) of polyVAc shifted to higher M_n values, with conversion without any noticeable tailing or shoulder formation (Figs. S19-S22), indicating good retention of chain-end functionality and negligible chain termination.

Controlled on–off light switching regulation of VAc polymerization using complexes **1**–**4** in the presence of TPO in CH_2Cl_2 was validated by

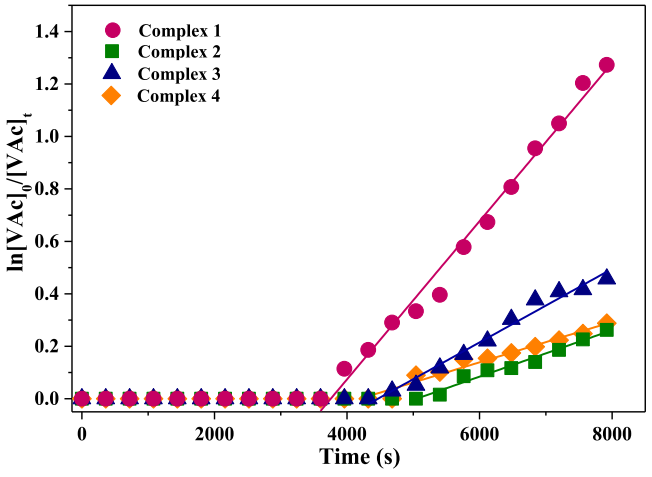

Fig. 5. Kinetics plot for the photoinduced polymerization of VAc with complexes **1**–**4**; [VAc]/[Ni^{II}]/[TPO] = 900/1.5/0.5 at 25 °C.

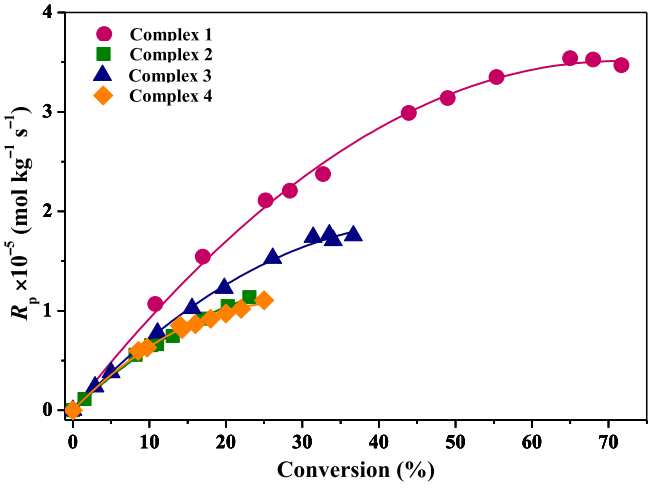

Fig. 6. Dependence of R_p values on VAc conversion with complexes **1**–**4**; [VAc]/[Ni^{II}]/[TPO] = 900/1.5/0.5 at 25 °C.

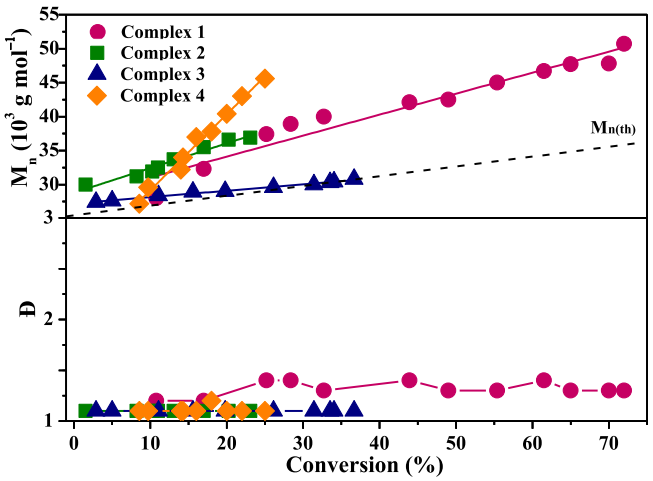

Fig 7. Dependence of M_n and Đ on the conversion for photo-OMRP of VAc with complexes **1**–**4**; [VAc]/[Ni^{II}]/[TPO] = 900/1.5/0.5 at 25 °C.

collecting enough polymer after a given period of irradiation and reinjecting it for the next cycle following a 1 h-on/1h-off LED irradiation in the photo-induced OMRP upon the induction period (Fig. 8). The lack of reaction in the dark suggested that the polymerization could be activated/deactivated by light leading to controlled regulation of the polymerization process. After removal of the light source, no further conversion was observed during the course of 1 h; however, re-exposure to light led to further reaction progress. This procedure could be repeated several times, indicating very efficient activation and deactivation of the polymerization process. These data indicate that when irradiation is removed from the system, the chain-ends are found as {Ni^{III}(VAc)} species, and upon re-exposure to irradiation in the presence of VAc, the chain-ends are efficiently and reversibly converting to propagating radicals and Ni^{II} species. Therefore, the control over the formation and termination of active species can be performed by using a simple on–off operation of light during nickel-photoinduced OMRP.

Computational studies were performed to evaluate the preferential photo-OMRP mechanism conducted by complexes **1**–**4**. Calculation attempts to perform single and double coupling between the monomer radical and the Ni^{II} complexes were successful. Structural optimization was conducted for complexes **1**–**4** and their respective species, {Ni^{III}(-VAc)} and {$Ni^{IV}(VAc)_2$}. The calculated thermodynamic parameters for the coupling between the Ni^{II} complex and monomer radical generated by the computational data assisted in indicating the major mechanism (Fig. 9). The photo-OMRP can occur under the reversible deactivation (RD) or degenerative transfer (DT) mechanism, the predominance of one mode over the other also depends on the nature and coordination sphere of the metal complex. The DFT calculations suggest that VAc polymerization mediated by complexes **1**–**4** is conducted by the RD mechanism, once the {Ni^{III}(VAc)} species bearing one vinyl radical are the most favorable from a thermodynamic viewpoint. (Table 2). For a possible DT mechanism, a second coupling of a propagating vinyl radical with the {Ni^{III}(VAc)} species must occur for an intermediate six-coordinate complex {$Ni^{IV}(VAc)_2$} be formed. For the latter case, the ΔG values are much more positive than those values for RD mechanism, that means the formation of the six-coordinate intermediate complex is less favorable.

Note that a significant deviation between experimental and calculated molecular weights for complexes **1**, **2** and **4** was obtained, because the incomplete conversion of Ni^{II} to organonickel species {Ni^{III}(VAc)},

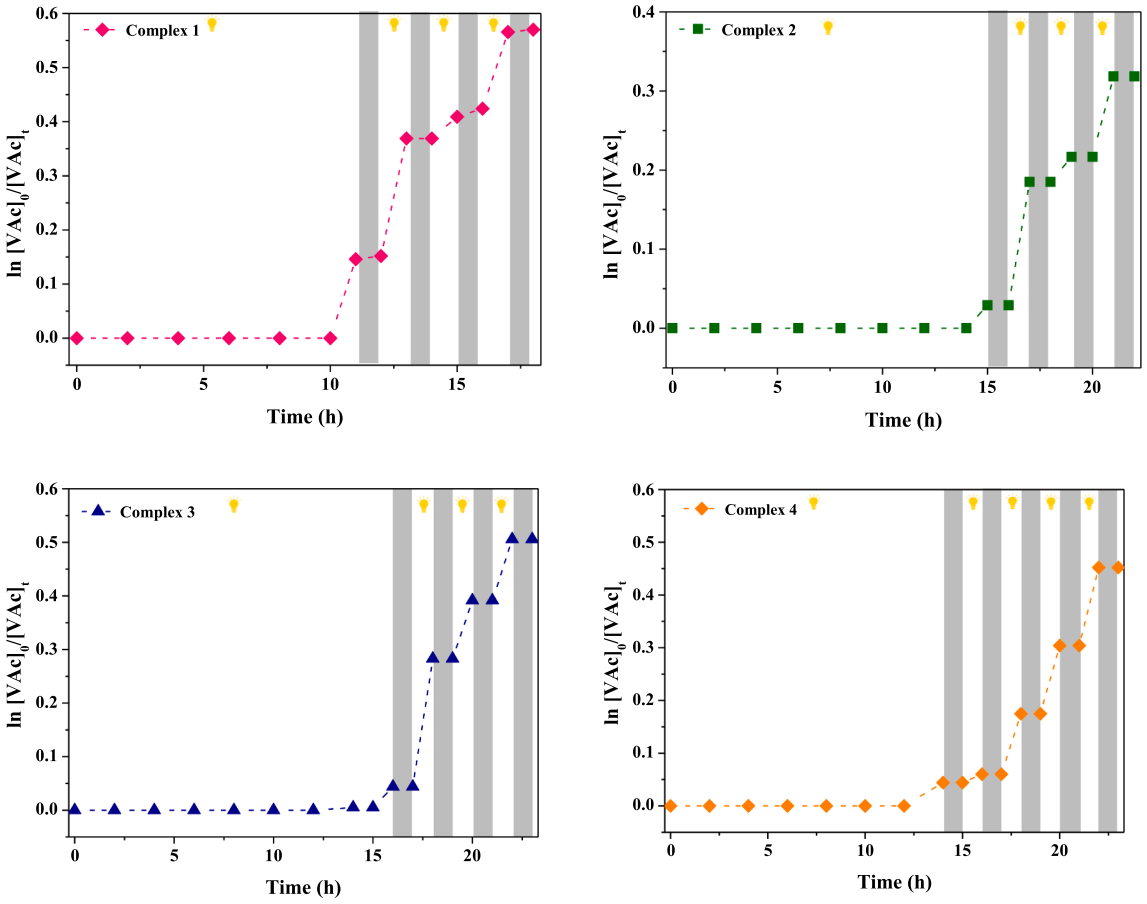

Fig. 8. On/off experiment for photo-OMRP using complexes **1**–**4** as mediators under [VAc]/[Ni^{II}]/[TPO] = 900/1.5/0.5 M ratio at 25 °C.

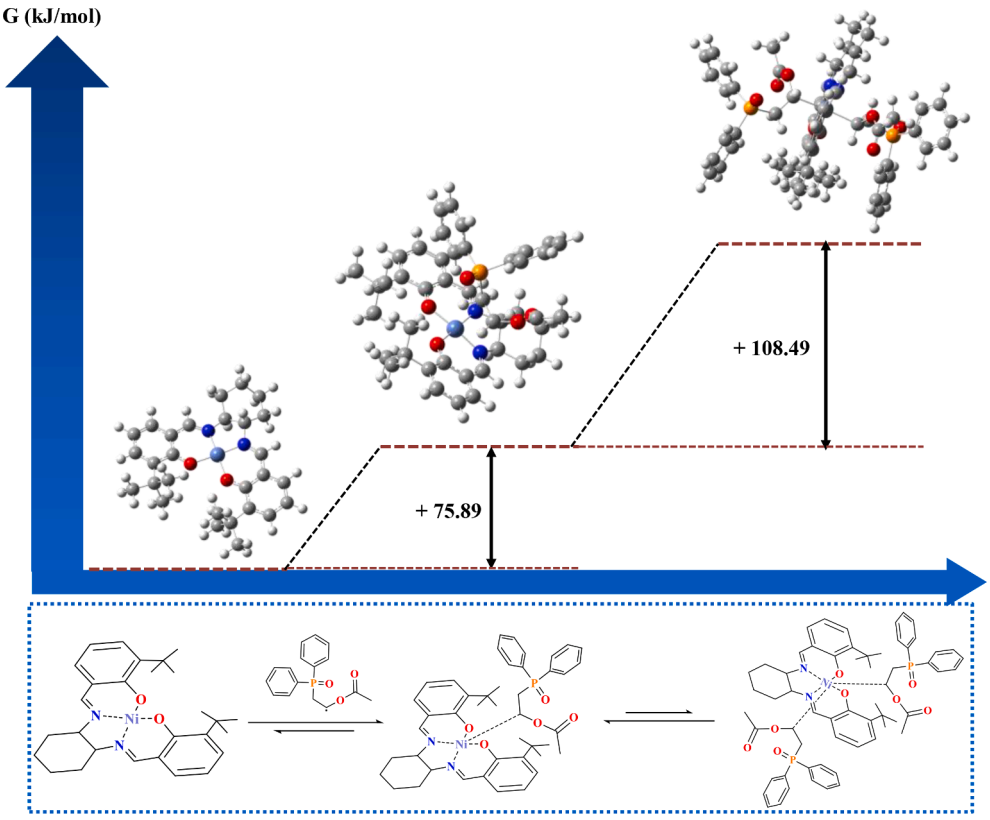

Fig. 9. Energy diagram and computational data for the photoinduced polymerization of VAc with complex **3**.

Table 2
Calculated thermodynamic parameters for the photoinduced polymerization of VAc with complexes **1**–**4**.

Complex	ΔG (kJ/mol) Ni^{III}(VAc)	ΔH (kJ/mol) Ni^{III}(VAc)	ΔG (kJ/mol) $Ni^{IV}(VAc)_2$	ΔH (kJ/mol) $Ni^{IV}(VAc)_2$	BDE[a]
1	59.27	6.04	105.94	12.58	−6.04
2	59.14	5.68	102.76	12.23	−5.68
3	75.89	−11.0	108.49	13.12	+11.0
4	64.98	4.32	97.31	14.30	−4.32

[a] Calculated Ni-C bond dissociation enthalpy for the exit of one radical from {Ni^{III}(VAc)}.

supported by Ni-C bond dissociation enthalpy (BDE) values. However, the positive BDE for complex **3** suggests that the {Ni^{III}(VAc)} species is more favored in the activation/deactivation equilibrium, since more energy is need to cleave Ni-C bond, and thus, maintaining the nickel as organonickel species and fulfilling the ideal assumption of one polymer chain per nickel.[54] Therefore, the experimental molecular weights were closer to theoretical values, indicating that a better control was reached for photo-OMRP of VAc with complex **3**.

2.9. Copolymerization of VAc and MA

To further demonstrate the living nature of this system, block copolymers of VAc and MA were synthesized using the sequential visible-light-induced process. Irradiation of VAc and 0.5 equiv. of TPO in the presence of complexes **1**–**4** afforded a well-defined macroinitiator {Ni^{III}(PVAc)} ($M_n \approx 12000$ g mol^{-1}, Đ = 1.1). Subsequent visible-light induced copolymerization with MA led to formation of desired block copolymers (Table 3). *SEC* traces of the block copolymers revealed a complete shift to higher molecular weight compared to the starting macroinitiator, and the amount of unreacted first block was negligible

Table 3
Synthesis of poly[VAc]-*b*-[MA] via photo-OMRP using complexes **1**–**4** as mediators under [VAc]/[Ni^{II}]/[TPO] = 900/1.5/0.5 M ratio at 25 °C.

Entry	Complex	$M_{n,GPC}$ (×10^3)	$M_{n,th}$[b] (×10^3)	Đ
1	**1**	67	54	1.4
2	**2**	50	45	1.2
3	**3**	54	39	1.2
4	**4**	62	41	1.2

[b] $M_{n,th} = M_n$(macroinitiator) + M_n (M) × ratio × conv(%).

(Fig. 10). The molecular weights of final block copolymers were close to the theoretical values with narrow polydispersity (Đ ≤ 1.4). The efficient block copolymerization confirmed the feature of living radical polymerization. Hence, this experiment indicates that the polymerizations were initiated using the {Ni^{III}(PVAc)} adduct that generated the radical initiator and the control agent upon photolysis as can be seen from Table 3 and Fig. 10.

3. Conclusions

The new complex **4** was successfully synthetized and fully characterized by UV–vis, FTIR, NMR and MALDI-TOF spectroscopy, elemental analysis, molar conductance, cyclic voltammetry, and computational methods. The photo-OMRP of VAc was successfully carried out using TPO as initiator under LED irradiation with complexes **1**–**4** using [VAc]/[Ni^{II}]/[TPO] = 900/1.5/0.5 M ratio at 25 °C. All complexes presented good control ability, where a linear increase in molecular weight with conversion and linear pseudo-first order kinetics were obtained. Nevertheless, the polymerization mediated by **3** showed the best control over molecular weight (M_n matching $M_{n,th}$) and dispersity (Đ < 1.5). Also, the BDE for complex **3** suggests that the {Ni^{III}(VAc)} species is more favored, since more energy is need to cleave this bond. The reversible deactivation is the major control pathway for the photo-

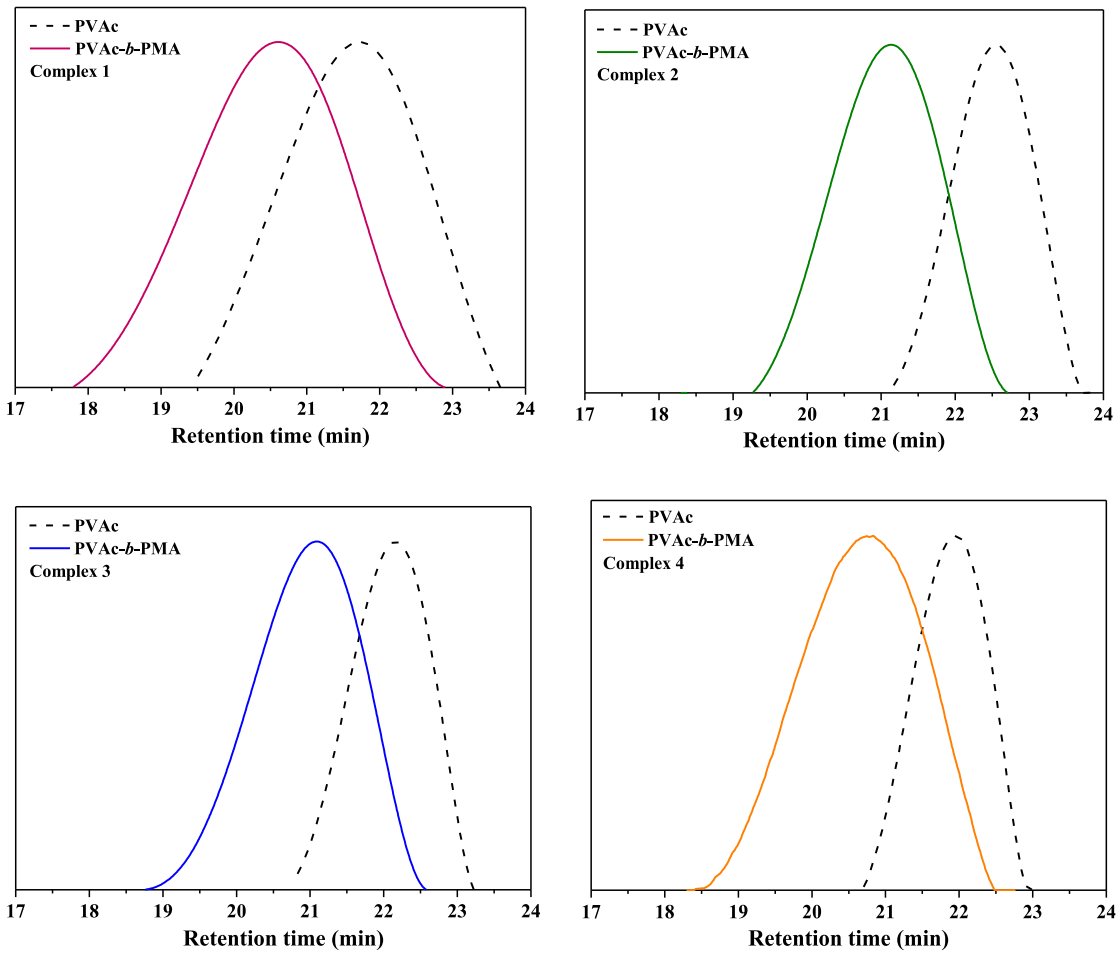

Fig. 10. GPC traces of the PVAc macroinitiator before and after block copolymerization with VAc and synthesis of poly[VAc]-*b*-[MA] using complexes **1**–**4** as mediators under [VAc]/[Ni^{II}]/[TPO] = 900/1.5/0.5 M ratio at 25 ℃.

OMRP of VAc mediated by the Ni^{II} complexes, as suggested by calculated thermodynamic data. The periodic light-on–off using the complexes **1**–**4** was repeated several times and no chain growth was observed during the light-off periods. Thus, in addition to controlling the initiation steps, LED irradiation also regulated the chain growth process by activating Ni–C bond in {Ni^{III}(PVAc)}. Efficient block copolymer synthesis under LED irradiation, further confirmed the versatile capability of these complexes **1**–**4** in photoinduced controlled/living radical polymerization [54].

CRediT authorship contribution statement

Naralyne M. Pesqueira: Methodology, Investigation, Funding. **Camila Bignardi:** Writing – original draft, Investigation. **Larissa F. Oliveira:** Investigation, Formal analysis. **Antonio E.H. Machado:** Methodology, Formal analysis. **Valdemiro P. Carvalho-Jr:** Writing – review & editing, Writing – original draft, Visualization, Validation, Funding acquisition, Formal analysis. **Beatriz E. Goi:** Supervised the project, conceived the study and were in charge of overall direction and planning.

Declaration of Competing Interest

The authors declare that they have no known competing financial interests or personal relationships that could have appeared to influence the work reported in this paper.

Data availability

No data was used for the research described in the article.

Acknowledgements

BEG, VPCJ and NMP are indebted to the financial support from FAPESP, grant #2018/19395-9, grant #2018/06340-1, and #2021/11741-8 respectively, São Paulo Research Foundation (FAPESP). AEHM is also indebted to the financial support of FAPEMIG (Proc. CEX - APQ-03017-16) and CNPq (Proc. 307443/2015-9). AEHM participated in this study during his stay as Visiting Professor at the Federal University of Goiás, Catalão, Goiás, Brazil, in the Graduate Program in Exact and Technological Sciences. The authors are grateful to Prof. Dra. Carla Cristina Schmitt Cavalheiro for the 400 MHz-NMR and MALDI-TOF analyses performed at the Instituto de Química de São Carlos from Universidade de São Paulo.

Appendix A. Supplementary data

Supplementary data to this article can be found online at https://doi.org/10.1016/j.jphotochem.2022.114443.

References

[1] A. Marathianos, E. Liarou, A. Anastasaki, R. Whitfield, M. Laurel, A.M. Wemyss, D. M. Haddleton, Photo-induced copper-RDRP in continuous flow without external deoxygenation, Polym. Chem. 10 (32) (2019) 4402–4406.

[2] J. Lalevee, J.-P. Fouassier (Eds.), Photopolymerisation Initiating Systems, Royal Society of Chemistry, England, 2018.

[3] C.-H. Peng, T.-Y. Yang, Y. Zhao, X. Fu, Reversible deactivation radical polymerization mediated by cobalt complexes: recent progress and perspectives, Org. Biomol. Chem. 12 (43) (2014) 8580–8587.

[4] M. Kaur, A.K. Srivastava, Photopolymerization: a review, J. Macromol. Sci., Part C Polym. Rev. 42 (2002) 481–512, https://doi.org/10.1081/mc-120015988.

[5] A. Ohtsuki, A. Goto, H. Kaji, Visible-light-induced reversible complexation mediated living radical polymerization of methacrylates with organic catalysts, Macromolecules 46 (1) (2013) 96–102.

[6] L.E.N. Allan, M.R. Perry, M.P. Shaver, Organometallic mediated radical polymerization, Progr. Polym. Sci. 37 (1) (2012) 127–156.

[7] K. Matyjaszewski, Introduction to living polymeriz. Living and/or controlled polymerization, J. Phys. Org. Chem. 8 (4) (1995) 197–207.

[8] J.-S. Wang, K. Matyjaszewski, Controlled/"living" radical polymerization. Atom transfer radical polymerization in the presence of transition-metal complexes, J. Am. Chem. Soc. 117 (20) (1995) 5614–5615.

[9] B.B. Wayland, L. Basickes, S. Mukerjee, M. Wei, M. Fryd, Living radical polymerization of acrylates Initiated and Controlled by organocobalt porphyrin complexes, Macromolecules 30 (26) (1997) 8109–8112.

[10] C. Detrembleur, D.-L. Versace, Y. Piette, M. Hurtgen, C. Jérôme, J. Lalevée, A. Debuigne, Synthetic and mechanistic inputs of photochemistry into the bisacetylacetonatocobalt-mediated radical polymerization of n-butyl acrylate and vinyl acetate, Polym. Chem. 3 (7) (2012) 1856–1866.

[11] X. Pan, M.A. Tasdelen, J. Laun, T. Junkers, Y. Yagci, K. Matyjaszewski, Photomediated controlled radical polymerization, Progr. Polym. Sci. 62 (2016) 73–125.

[12] F.A. Leibfarth, et al., External regulation of controlled polymerizations, Angew. Chem. 52 (2013) 199–210, https://doi.org/10.1002/anie.201206476.

[13] Y. Zhao, M. Yu, S. Zhang, Z. Wu, Y. Liu, C.-H. Peng, X. Fu, A well-defined, versatile photoinitiator (Salen)Co–CO2CH3 for visible light-initiated living/controlled radical polymerization, Chem. Sci 6 (5) (2015) 2979–2988.

[14] S. Banerjee, V. Ladmiral, A. Debuigne, C. Detrembleur, R. Poli, B. Améduri, Organometallic-mediated radical polymerization of vinylidene fluoride, Angew. Chem. 57 (11) (2018) 2934–2937.

[15] P. Rinaldo, Radical coordination chemistry and its relevance to metal-mediated radical polymerization, Eur. J. Inorg. Chem. 10 (2011) 1513–1530, https://doi.org/10.1002/ejic.201001364.

[16] A. Debuigne, R. Poli, C. Jérôme, R. Jérôme, C. Detrembleur, Overview of cobalt-mediated radical polymerization: Roots, state of the art and future prospects, Progr. Polym. Sci. 34 (3) (2009) 211–239.

[17] R. Poli, L.E.N. Allan, M.P. Shaver, Iron-mediated reversible deactivation controlled radical polymerization, Progr. Polym. Sci. 39 (10) (2014) 1827–1845.

[18] E. Le Grognec, et al., Radical polymerization of styrene controlled by half-sandwich Mo(III)/Mo(IV) couples: all basic mechanisms are possible, J. Am. Chem. Soc. 123 (2001) 9513–9524, https://doi.org/10.1021/ja010998d.

[19] B.B. Wayland, G. Poszmik, M. Fryd, Metalloradical reactions of rhodium(II) porphyrins with acrylates: reduction, coupling, and photopromoted polymerization, Organometallics 11 (11) (1992) 3534–3542.

[20] R. Mazzoni, F. Roncaglia, L. Rigamonti, When the metal makes the difference: template syntheses of tridentate and tetradentate Salen-type schiff base ligands and related complexes, Crystals 11 (5) (2021) 483.

[21] B.A. Riga, M.D. Neves, A.E.H. Machado, D.M.S. Araújo, J.R. Souza, O. R. Nascimento, V.T. Santana, C.C.S. Cavalheiro, V.P. Carvalho-Jr, B.E. Goi, Synthesis of cobalt(II)-α-diimines complexes and their activity as mediators in organometallic mediated radical polymerization of vinyl acetate, Inorg. Chim. Acta 471 (2018) 620–629.

[22] W. Al Zoubi, Y.G. Ko, Organometallic complexes of Schiff bases: Recent progress in oxidation catalysis, J. Organomet. Chem. 822 (2016) 173–188.

[23] Z. Beigi, A.H. Kianfar, H. Farrokhpour, M. Roushani, M.H. Azarian, W.A. K. Mahmood, Synthesis, characterization and spectroscopic studies of nickel (II) complexes with some tridentate ONN donor Schiff bases and their electrocatalytic application for oxidation of methanol, J. Mol. Liq. 249 (2018) 117–125.

[24] Y. Zou, et al. Asymmetric synthesis of tailor-made amino acids using chiral Ni(II) complexes of Schiff bases. An update of the recent literature. Molecules, 25(2020), 2739. doi: 10.3390/molecules25122739.

[25] M.F.S. Teixeira, T.R.L. Dadamos, An electrochemical sensor for dipyrone determination based on nickel-salen film modified electrode, Procedia Chem. 1 (2009) 297–300, https://doi.org/10.1016/j.proche.2009.07.074.

[26] C-B. Li, et al. Photocatalytic hydrogen production based on a serial metal-salen complexes and the reaction mechanism. ChemCatChem, 11(2019), 6324–6331, doi: 10.1002/cctc.201901656.

[27] F. Thomas, Ligand-centred oxidative chemistry in sterically hindered Salen complexes: An interesting case with nickel, Dalton trans. 45 (2016) 10866–10877, https://doi.org/10.1039/c6dt00942e.

[28] T.T. Silva, Y.F. Silva, A.E.H. Machado, P.I.S. Maia, C.R.B. Tasso, B.S. Lima-Neto, J. L. Silva Sá, V.P. Carvalho-Jr, N.C. Batista, B.E. Goi, Cycloalkyl-substituted salicylaldimine-nickel(II) complexes as mediators in controlled radical polymerization of vinyl acetate, J. Macromol. Sci., Part A: Pure Appl. Chem. 56 (12) (2019) 1132–1140.

[29] Y.F. Silva, B.A. Riga, V.M. Deflon, J.R. Souza, L.H.F. Silva, A.E.H. Machado, P.I. S. Maia, C.-J. Valdemiro P., B.E. Goi, Organometallic-mediated radical polymerization using well-defined Schiff base cobalt(II) complexes, J. Coord. Chem. 71 (22) (2018) 3776–3789.

[30] B. A. Riga, et al. Cobalt(II) complexes of α-diimine derived from cycloalkylamines as controlling agents for organometallic mediated radical polymerization of vinyl acetate. Polyhedron, 192(2020), 114870. doi: 10.1016/j.poly.2020.114870.

[31] P.K. Hashimoto, et al., Manganese(Ii) Schiff-base-mediated reversible deactivation controlled radical polymerization of vinyl acetate, New J. Chem. 45 (2021) 10109–10117, https://doi.org/10.1039/d1nj00493j.

[32] L.F. Oliveira, et al., Photocontrolled reversible-deactivation radical polymerization of butyl acrylate mediated by Salen-type Co^{II} complexes, Eur. Polym. J. 159 (2021), 110757, https://doi.org/10.1016/j.eurpolymj.2021.110757.

[33] C. Bignardi, et al., Photoinduced organometallic mediating radical polymerization of acrylates mediated by CoII complexes of non-symmetrical tetradentate Schiff-base ligands, J. Photochem. Photobiol. A: Chem. 423 (2022), 113595, https://doi.org/10.1016/j.jphotochem.2021.113595.

[34] N.U. Hofsløkken, L. Skattebøl, F. Johansson, S.K. Bertilsson, P.G. Andersson, J. Møller, A. Senning, X.-K. Yao, H.-G. Wang, J.-P. Tuchagues, M. Ögren, Convenient Method for the ortho-formylation of phenols, Acta Chem. Scand. 53 (1999) 258–262.

[35] D. Tomczyk, L. Nowak, W. Bukowski, K. Bester, P. Urbaniak, G. Andrijewski, B. Olejniczak, Reductive and oxidative electrochemical study and spectroscopic properties of nickel(II) complexes with N_2O_2 Schiff bases derived from (±)-trans-N, N′-bis(salicylidene)-1,2-cyclohexanediamine, Electrochim. Acta 121 (2014) 64–77.

[36] B. Wang, D. Gong, G. Wu, X. Zhang, Polymerization of 1,3-butadiene using (salen) Ni(II) and (salphen)Ni(II) complexes in combination with methylaluminoxane, e-Polymers 12 (1) (2012), https://doi.org/10.1515/epoly.2012.12.1.777.

[37] D. Vanderveer, M.L. Colón, X.R. Bu, Crystal structure of a chiral Ni complex: (R, R)-N, N'-bis(3-t-butylsalicylidene)-1,2-cyclohexanediaminonickel(II), Anal. Sci. 18 (11) (2002) 1283–1284.

[38] S. Stoll, A. Schweiger, EasySpin, a comprehensive software package for spectral simulation and analysis in EPR, J. Magn. Reson. 178 (1) (2006) 42–55.

[39] C. Adamo, V. Barone, Toward reliable density functional methods without adjustable parameters: The PBE0 model, J. Chem. Phys. 110 (13) (1999) 6158–6170.

[40] M. J. Frisch, G. W. Trucks, H. B. Schlegel, G. E. Scuseria, M. A. Robb, J. R. Cheeseman, G. Scalmani, V. Barone, B. Mennucci, G. A. Petersson, H. Nakatsuji, M. Caricato, X. Li, H. P. Hratchian, A. F. Izmaylov, J. Bloino, G. Zheng, J. L. Sonnenberg, M. Hada, M. Ehara, K. Toyota, R. Fukuda, J. Hasegawa, M. Ishida, T. Nakajima, Y. Honda, O. Kitao, H. Nakai, T. Vreven, J. A. Montgomery, Jr., J. E. Peralta, F. Ogliaro, M. Bearpark, J. J. Heyd, E. Brothers, K. N. Kudin, V. N. Staroverov, T. Keith, R. Kobayashi, J. Normand, K. Raghavachari, A. Rendell, J. C. Burant, S. S. Iyengar, J. Tomasi, M. Cossi, N. Rega, J. M. Millam, M. Klene, J. E. Knox, J. B. Cross, V. Bakken, C. Adamo, J. Jaramillo, R. Gomperts, R. E. Stratmann, O. Yazyev, A. J. Austin, R. Cammi, C. Pomelli, J. W. Ochterski, R. L. Martin, K. Morokuma, V. G. Zakrzewski, G. A. Voth, P. Salvador, J. J. Dannenberg, S. Dapprich, A.D. Daniels, O. Farkas, J.B. Foresman, J.V. Ortiz, J. Cioslowski, D. J. Fox, G09: Gaussian 09, Revision E.01. Gaussian, Inc., Wallingford, CT. 2015.

[41] N. Godbout, D.R. Salahub, J. Andzelm, E. Wimmer, Optimization of Gaussian-type basis sets for local spin density functional calculations. Part I. Boron through neon, optimization technique and validation, Can. J. Chem. 70 (2) (1992) 560–571.

[42] P. Mukherjee, C. Biswas, M.G.B. Drew, A. Ghosh, Structural variations in Ni(II) complexes of salen type di-Schiff base ligands, Polyhedron 26 (13) (2007) 3121–3128.

[43] D. Tomczyk, et al., The mechanism of electropolymerization of nickel(II) salen type complexes, New J. Chem. 41 (2017) 2112–2123, https://doi.org/10.1039/c6nj03635j.

[44] M. Murrie, Cobalt(ii) single-molecule magnets, Chem. Soc. Rev. 39 (2010) 1986–1995, https://doi.org/10.1039/B913279C.

[45] A.N. Morin, C. Detrembleur, C. Jérôme, P. De Tullio, R. Poli, A. Debuigne, Effect of head-to-head addition in vinyl acetate controlled radical polymerization: why is Co (acac)2-mediated polymerization so much better? Macromolecules 46 (11) (2013) 4303–4312.

[46] S. Maria, H. Kaneyoshi, K. Matyjaszewski, R. Poli, Effect of electron donors on the radical polymerization of vinyl acetate mediated by $[Co(acac)_2]$: degenerative transfer versus reversible homolytic cleavage of an organocobalt(III) complex, Chem. Eur. J. 13 (9) (2007) 2480–2492.

[47] S. Li, B.d. Bruin, C.-H. Peng, M. Fryd, B.B. Wayland, Exchange of organic radicals with organo-cobalt complexes formed in the living radical polymerization of vinyl acetate, J. Am. Chem. Soc. 130 (40) (2008) 13373–13381.

[48] A. Debuigne, A.N. Morin, A. Kermagoret, Y. Piette, C. Detrembleur, C. Jérôme, R. Poli, Key role of intramolecular metal chelation and hydrogen bonding in the cobalt-mediated radical polymerization of N-vinyl amides, Chem. Eur. J. 18 (40) (2012) 12834–12844.

[49] Y. Piette, A. Debuigne, C. Jérôme, V. Bodart, R. Poli, C. Detrembleur, Cobalt-mediated radical (co)polymerization of vinyl chloride and vinyl acetate, Polym. Chem. 3 (10) (2012) 2880.

[50] G. Ceyhan, M. Köse, V. McKee, S. Uruş, A. Gölcü, M. Tümer, Tetradentate Schiff base ligands and their complexes: synthesis, structural characterization, thermal, electrochemical and alkane oxidation, Spectrochim. Acta A Mol. Biomol. 95 (2012) 382–398.

[51] B.S. Garg, D. N. Kumar. Spectral studies of complexes of nickel(II) with tetradentate schiff bases having N_2O_2 donor groups. Spectrochim. Acta Part A, 59 (2003) 229-234. doi: 10.1016/s1386-1425(02)00142-7.

[52] D.F. Back, G.M. de Oliveira, L.A. Fontana, B.F. Ramão, D. Roman, B.A. Iglesias, One-pot synthesis, structural characterization, UV–Vis and electrochemical

analyses of new Schiff base complexes of Fe(III), Ni(II) and Cu(II), J. Mol. Struct. 1100 (2015) 264–271.

[53] N. Raman, et al., Redox and antimicrobial studies of transition metal(II) tetradentate Schiff base complexes, Transit. Met. Chem. 28 (2003) 29–36, https://doi.org/10.1023/A:1022544126607.

[54] M. Wakioka, K.-Y. Baek, T. Ando, M. Kamigaito, M. Sawamoto, Possibility of living radical polymerization of vinyl acetate catalyzed by iron(I) complex, Macromolecules 35 (2) (2002) 330–333.